A Framework for Simulating the Tropical Cyclone Boundary Layer Using Large-Eddy Simulation and Its Use in Evaluating PBL Parameterizations

XIAOMIN CHEN,[a] GEORGE H. BRYAN,[b] JUN A. ZHANG,[a,c] JOSEPH J. CIONE,[a] AND FRANK D. MARKS[a]

[a] *NOAA/AOML/Hurricane Research Division, Miami, Florida*
[b] *National Center for Atmospheric Research, Boulder, Colorado*
[c] *Cooperative Institute for Marine and Atmospheric Studies, University of Miami, Miami, Florida*

(Manuscript received 27 July 2020, in final form 21 August 2021)

ABSTRACT: Boundary layer turbulent processes affect tropical cyclone (TC) structure and intensity change. However, uncertainties in the parameterization of the planetary boundary layer (PBL) under high-wind conditions remain challenging, mostly due to limited observations. This study presents and evaluates a framework of numerical simulation that can be used for a small-domain [$O(5)$-km] large-eddy simulation (LES) and single-column modeling (SCM) to study the TC boundary layer. The framework builds upon a previous study that uses a few input parameters to represent the TC vortex and adds a simple nudging term for temperature and moisture to account for the complex thermodynamic processes in TCs. The reference thermodynamic profiles at different wind speeds are retrieved from a composite analysis of dropsonde observations of mature hurricanes. Results from LES show that most of the turbulence kinetic energy and vertical momentum flux is associated with resolved processes when horizontal grid spacing is $O(10)$ m. Comparison to observations of turbulence variables such as momentum flux, effective eddy viscosity, and turbulence length scale show that LES produces reasonable results but highlight areas where further observations are necessary. LES results also demonstrate that compared to a classic Ekman-type boundary layer, the TC boundary layer is shallower, develops steady conditions much quicker, and exhibits stronger wind speed near the surface. The utility of this framework is further highlighted by evaluating a first-order PBL parameterization, suggesting that an asymptotic turbulence length scale of 40 m produces a good match to LES results.

KEYWORDS: Boundary layer; Hurricanes/typhoons; Large eddy simulations; Numerical analysis/modeling; Parameterization; Single column models; Subgrid-scale processes

1. Introduction

The tropical cyclone (TC) boundary layer is distinct from the daytime convective boundary layer due to the effect of the cyclone's rotation on the boundary layer height and turbulence characteristics (Eliassen 1971). Turbulent mixing processes in the TC boundary layer are important contributors to the cyclone's intensity change since it controls the depth and strength of radial inflow (Foster 2009; Zhang et al. 2015; Zhang and Pu 2017). Specifically, the inflow strength is closely tied to a boundary layer spinup paradigm of TCs (Smith and Montgomery 2015), in which the increase of the maximum tangential wind in the boundary layer occurs if the inflow is strong enough such that the fractional rate of reduction of inward displacement for an air parcel is more than the fractional rate of reduction of absolute angular momentum due to the frictional torque. Turbulence processes also affect TC size and structure by modulating the boundary layer moisture and convective activity in the outer core region (Bu et al. 2017).

However, due to safety and practical considerations it should be noted that direct in situ flux measurements in the TC boundary layer are rare. Most values are available in the outer region of TC circulations where the surface wind is relatively weak (18–30 m s^{-1}; French et al. 2007, hereafter F07; Zhang and Drennan 2012). Although recent measurements have been obtained using drones in the eyewall of major hurricanes (Cione et al. 2020, hereafter C20), it remains very rare to have observations from the surface layer ($z < \sim 100$ m) in hurricane-force winds. The scarce observations limit our understanding toward the turbulence characteristics in the TC boundary layer, which further impedes the development of planetary boundary layer (PBL) parameterizations in TC conditions. Moreover, the existing PBL parameterization schemes have generally been developed for conditions over land, or for weak winds over oceans, and directly applying these PBL schemes in high-wind conditions (like TCs) demands a closer examination.

In recognition of these issues, several studies have used large-eddy simulation (LES) to provide insight into the TC boundary layer (e.g., Zhu 2008; Rotunno et al. 2009; Green and Zhang 2015; Stern and Bryan 2018; Wu et al. 2018; Li and Pu 2021). In LES, turbulent eddies are resolved explicitly using grid spacing of $O(100)$ m or less, and a PBL parameterization is not used. However, because TCs are so large, spanning several hundred kilometers horizontally, it can be very computationally expensive to simulate an entire TC with eddy-resolving grid spacing.

With these points in mind, a modeling framework tailored to the TC boundary layer is presented in this study that can be used for multiple purposes, including to understand the turbulence characteristics in hurricane conditions, and to assess the performance of various PBL schemes and uncertainties in the parameterizations of boundary layer processes. The framework builds upon a simple method of simulating boundary layer winds of TCs

Corresponding author: Xiaomin Chen, xiaomin.chen@noaa.gov

DOI: 10.1175/JAS-D-20-0227.1

TABLE 1. A list of category 4–5 hurricanes from 1999 to 2010 in the dropsonde dataset. "No. of total sondes" refers to the number of sondes from all flights for a given storm.

Year	Storm name	No. of total dropsondes
1999	Floyd	33
2003	Fabian	43
2003	Isabel	135
2004	Frances	57
2004	Ivan	141
2005	Dennis	8
2005	Katrina	17
2005	Rita	87
2007	Dean	19
2008	Gustav	6
2010	Earl	24

(Bryan et al. 2017, hereafter B17), which can be used for LES and also single-column modeling (SCM) that can use different PBL schemes. An important addition to this framework is the use of composite in situ thermodynamic data from dropsondes released in mature hurricanes as a reference profile, and the averaged thermodynamic profiles in the modeling framework are held nearly fixed by applying a "large-scale" nudging to these profiles. The kinematic profiles are allowed to evolve using the "mesoscale tendency" terms of B17 that account for the mesoscale pressure-gradient and centrifugal accelerations. The thermodynamic nudging allows for a simple but accurate approach to model the TC boundary layer because it circumvents the need to specify multiple complex processes such as radiation, large-scale subsidence, and microphysical processes that influence thermodynamic profiles in TCs. Output from LES can be used as a benchmark to evaluate PBL parameterizations in high-wind conditions, as demonstrated for one PBL scheme herein.

The remainder of the paper is organized as follows. Section 2 presents a composite analysis of dropsonde observations that provides the reference thermodynamic profiles used in this study. The modeling framework tailored to the TC boundary layer as well as the model setup for LES and SCM using a PBL scheme are introduced in section 3. Analyses of LES output and verification of LES results against observations are presented in section 4. The differences between a TC boundary layer and an "ordinary" shear-driven, Ekman-type boundary layer are examined in section 5. In section 6, the LES results are used to evaluate a first-order PBL scheme in TC conditions. Concluding remarks are provided in section 7.

2. Observations

a. Composite profiles for category 4–5 hurricanes

To determine average profiles in high-wind conditions of TCs to guide this study, we perform a composite analysis of dropsonde data collected during research and operational flights conducted by NOAA P3 and G-IV, NASA DC-8 and G-V, and Air Force C130 aircrafts in category 4–5 hurricanes from 1999 to 2010. The GPS dropsonde observing platform records measurements of air temperature, relative humidity, pressure, and horizontal and vertical wind speeds. Detailed instrument documentation for the dropsonde can be found in Hock and Franklin (1999). After rigorous quality control using NCAR's Atmospheric Sounding Processing Environment (ASPEN) software along with additional manual inspection, the dataset used in this study includes observations from 570 dropsondes that were collected in 11 category 4–5 hurricanes (see Table 1).

The dropsonde data are grouped as a function of the normalized radius, which is defined as the radius to the vortex center (r) normalized by the radius of maximum wind (RMW; i.e., $r^* = r/\text{RMW}$) following Zhang et al. (2011b). Figures 1a and 1b show the radius–height plots for the composite tangential and radial winds. The RMW of the composite vortex is set to 30 km, which is approximately the mean value indicated by the stepped-frequency microwave radiometer (SFMR) and flight-level wind data (Zhang et al. 2013). The composite vortex has a maximum tangential wind of $\sim 65\,\text{m s}^{-1}$ near the RMW at roughly 500–600-m height. The boundary layer inflow is strongest outside the RMW, decelerates toward the RMW, and turns into outflow above ~1 km inside the RMW. These characteristics are similar to the boundary layer structures of simulated mature hurricanes (e.g., Kepert 2001; Nolan et al. 2009) and observational composites from Zhang et al. (2011b). The vertical profiles of tangential wind, radial wind, potential temperature, and mixing ratio of water vapor are extracted where the 10-m tangential wind is roughly $25\,\text{m s}^{-1}$ (V25 hereafter), $35\,\text{m s}^{-1}$ (V35 hereafter), and $45\,\text{m s}^{-1}$ (V45 hereafter) (Figs. 1c–f). The vertical profiles show that the boundary layer of mature hurricanes is generally statically stable in terms of potential temperature (Fig. 1e) or virtual potential temperature (not shown) under high-wind conditions, except for a very shallow (<100 m) statically unstable layer near the surface in V25 and V35.

b. Turbulence observations for evaluation of LES

Observations of vertical turbulence momentum flux τ from aircrafts in TCs come from F07, Zhang et al. (2011a, hereafter Z11), and C20. The flux data in F07 are from measurements in the rain-free outer region of category 4–5 hurricanes where the surface wind is relatively weak ($18–30\,\text{m s}^{-1}$). In comparison, the flux data in Z11 were collected in category 4–5 hurricanes before and during the eyewall penetrations by NOAA P3 aircrafts. The flux data in C20 were collected by a small unmanned aircraft system (sUAS), mostly in the eyewall of Hurricanes Maria (2017) and Michael (2018). Observational estimates of effective eddy diffusivity K and turbulence length scale l come from Zhang and Drennan (2012). Although there are only 68 measurements of K and l, and all of them are from tropical storm–force conditions, these data are nonetheless crucial for establishing the reliability of this modeling framework.

3. Modeling methodology

a. Framework to account for large-scale kinematic processes

The modeling framework is an extension of the "simple" method for simulating boundary layer winds in TCs that was first presented by B17 and was evaluated by Worsnop et al. (2017).

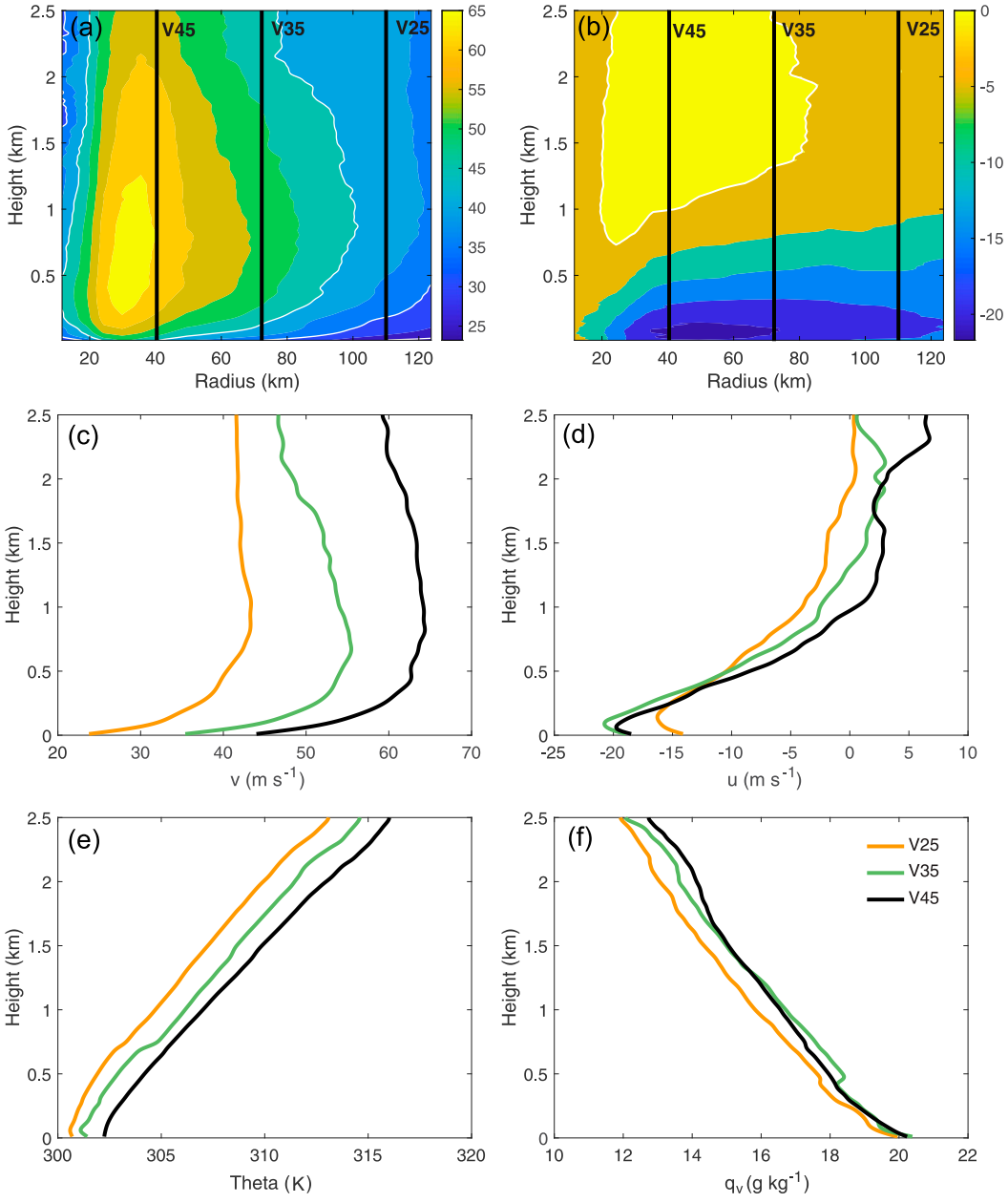

FIG. 1. (top) Radius–height plot of the composite (a) tangential and (b) radial winds in the lowest 2.5 km. The vertical lines with the text V45, V35, and V25 mark the location where the 10-m tangential wind is roughly 45, 35, and 25 m s^{-1}, respectively. (middle),(bottom) The vertical profiles for (c) tangential wind (m s^{-1}), (d) radial wind (m s^{-1}), (e) potential temperature (K), and (f) specific humidity (g kg^{-1}) for V45, V35, and V25, using colors as indicated by the legend in (f).

The primary idea is to account for large-scale conditions via specified values for gradient wind speed V, its radial gradient $\partial V/\partial r$, and a characteristic distance from the TC center R, as illustrated in Fig. 2. The primary merit of this approach is that it allows for controlled conditions without potentially complex feedback to the large-scale TC vortex. For example, in SCM using different PBL parameterizations, one can ensure that the simulations proceed under the same specified kinematic and thermodynamic conditions, thus ensuring a clean comparison of PBL schemes and allowing for a direct analysis of the effects of small-scale turbulence processes.

Another benefit of this approach is it allows for LES with a relatively small domain of $O(5)$ km, and thus grid spacing of $O(10)$ m can be used with present-day computing systems. This LES setup is much more computationally tractable than simulating an entire TC that spans several hundred kilometers

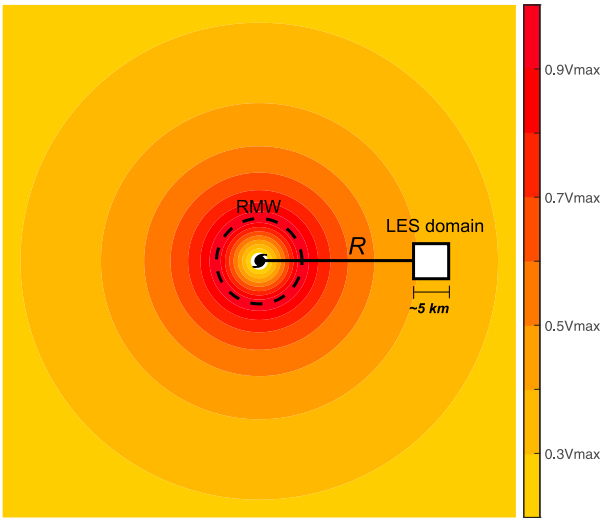

FIG. 2. The conceptual schematic of the LES modeling framework. The LES domain, shown as a white box, is located due east of the storm center (hurricane symbol) at a distance of R. Color shading denotes the near-surface tangential wind and the maximum tangential wind (Vmax) at the RMW is marked by a black dashed circle.

horizontally. Downsides of this approach include the inability to account for certain mesoscale processes, such as rainbands. It is also not possible to study rapidly evolving conditions, including TC intensification and decay. Thus, the framework clearly cannot address all types of TC boundary layers. However, the benefits of this approach include the ability to use high resolution (e.g., 10-m grid spacing) and modest supercomputing resources, and the ability to compare different modeling assumptions (e.g., different PBL schemes) in controlled and consistent conditions.

This approach of using a domain of horizontal extent of $O(5)$ km also mimics a single grid point in a mesoscale model. PBL parameterizations in mesoscale models act only on a vertical column of information (e.g., winds and thermodynamics variables) and the SCM approach here essentially reproduces what is occurring at a single grid point in an NWP model.

In this framework, the tangential velocity outside the radius of maximum wind is assumed to be a function of radius r according to the power law, i.e., $V_T = V(R/r)^n$, a concept similar to the modified Rankine vortex (e.g., Hughes 1952; Mallen et al. 2005; Chen et al. 2013). In this case, $\partial V_T/\partial r = -n(V/R)$ at $r = R$. Furthermore, although Fig. 2 illustrates a circularly symmetric TC (for simplicity), it is possible to account for different conditions in various quadrants of a TC with this framework. For example, one could run this modeling framework twice, with the same values of R and n but different values of V to account for a TC with varying winds in different regions of a TC.

Here, we set the reference gradient wind V based on the maximum tangential wind speed in the 500–1000 m layer from the dropsonde composites at different R (Figs. 1c,d), where R is determined from the radius–height dropsonde composites (see Figs. 1a,b). Table 2 shows the detailed information for three sets of experiments at different 10-m tangential wind, i.e., V25, V35, and V45, respectively. The value of n is chosen such that the simulated wind profiles at steady state best match the dropsonde composites. In our experiments n is set to a value slightly exceeding the range of the observations for mature hurricanes, i.e., n = 0.18–0.67, in Mallen et al. (2005). However, one difference should be noted: the observed n in Mallen et al. (2005) is related to the flight-level (~700 hPa) tangential winds while n in our setting is related to the tangential winds near the top of the boundary layer (~1 km).

TABLE 2. The input parameters for the LESs and single-column model simulations for V25, V35, and V45 experiments. V is gradient wind speed, R is radius from storm center, and n is a radial decay parameter, as described in the text.

Parameter	V25	V35	V45
V (m s^{-1})	44	58	65
R (km)	110	75	40
n (–)	0.7	0.7	0.75

b. *Framework to account for large-scale thermodynamic processes*

The original B17 method essentially neglected the effects of thermodynamics to focus only on wind profiles in TCs. In fact, moisture was neglected completely in B17, and the potential-temperature profile was nearly neutral throughout the PBL after a few hours of simulation. To overcome these limitations, but still retain the spirit of a ''simple'' technique that does not require a long list of inputs such as radiative and microphysical tendencies, herein we add a domainwide nudging term toward specified vertical profiles of potential temperature and specific humidity:

$$\frac{\partial \theta}{\partial t} = \cdots + \frac{\theta_r(z) - \langle\theta\rangle(z)}{\tau_n}, \tag{1a}$$

$$\frac{\partial q}{\partial t} = \cdots + \frac{q_r(z) - \langle q\rangle(z)}{\tau_n}, \tag{1b}$$

where θ is potential temperature, q is water vapor mixing ratio, the subscript r refers to a one-dimensional reference profile, angle brackets denote domain averages at a specified height, and τ_n is a nudging time scale. These tendencies are a function of height only, and are applied to every column in the domain; this approach ensures there are no horizontal gradients in tendencies to buoyancy that would alter thermal-wind balance. As noted earlier, this technique acts to ''anchor'' the thermodynamic state to that in actual major hurricanes, and allows us to bypass the specification of complex processes such as microphysics, radiation, large-scale horizontal advection, and large-scale subsidence.

For simulations herein, the profiles shown in Figs. 1e and 1f are used as the reference profiles. The default nudging time scale is 5 min; using a shorter nudging time scale does not affect the vertical profiles of turbulence fields (not shown), and a

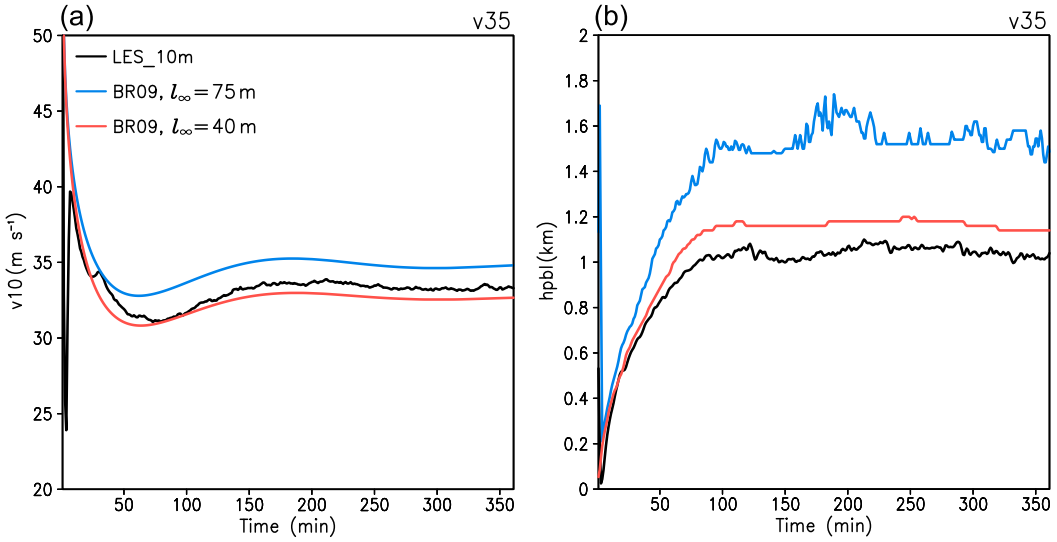

FIG. 3. Evolution of (a) the 10-m tangential wind speed and (b) boundary layer height for V35 from the LES (black, domain-averaged) and from the SCM simulation that uses BR09 with an asymptotic length scale $l_\infty = 75$ m (blue) and 40 m (red). The definition of boundary layer height is described in section 3d.

larger time scale is insufficient to maintain observed thermodynamic profiles.

c. *Details of simulations*

Cloud Model 1 (CM1; Bryan and Fritsch 2002) is used in this study for all simulations, including both LES and SCM. The primary advantage of LES, of course, is that the largest turbulent eddies can be explicitly resolved, and only the smaller subgrid-scale eddies are parameterized. For this study, subgrid-scale processes for LES are parameterized using a two-part LES subgrid model following the appendix in B17, which uses a standard turbulence kinetic energy (TKE)-based scheme following Deardorff (1980) at every grid point, and a term following Sullivan et al. (1994) that acts on horizontal velocities for $z < 100$ m to prevent excessive shear near the surface.

The initial thermodynamic conditions (potential temperature and water vapor mixing ratio) are shown in Figs. 1e and 1f. The sea surface temperature is set to be about 2°C warmer than the near-surface air temperature. This value of air–sea temperature difference is similar to the observed climatological value in hurricane conditions (Cione et al. 2000; Cione 2015). All simulations are run for 6 h and a quasi-steady state is reached after approximately 2.5 h (see one example using V35 in Fig. 3).

For LES we use 512 × 512 grid points horizontally and a horizontal grid spacing (Δx) of 10 m. Of note, the domain-averaged wind profiles and turbulence properties examined here are consistent when a larger LES domain [i.e., $O(10)$ km or $O(20)$ km] is used (not shown). In the vertical, there are 512 grid points, with a domain depth of 3 km. The vertical grid spacing is 5 m below 2 km and increases to 12.5 m between 2 and 3 km. Rayleigh damping is applied above 2 km for horizontal winds, vertical velocity, and perturbations of potential temperature, to damp vertically propagating gravity waves. Periodic boundary conditions are used in both horizontal directions.

For SCM simulations, a very similar model setup is used except that there is only a single column and the vertical grid spacing is 50 m. The LES subgrid turbulence model is turned off and a PBL parameterization is used instead to account for all turbulent processes. The PBL scheme of Bryan and Rotunno (2009, hereafter BR09), as modified by B17, is used for all SCM simulations in this paper.

To reduce the sensitivity of the results to surface layer parameterizations, as noted in earlier studies (Braun and Tao 2000; Smith and Thomsen 2010), the GFDL surface layer scheme (Kurihara and Tuleya 1974) from HWRF is used for all of the LESs and SCM simulations. The surface drag coefficient (C_d) and surface enthalpy exchange coefficient (C_k) in the GFDL surface layer scheme have been modified in recent years based on observations in hurricanes. Figure 4 shows C_d and C_k under neutral conditions as a function of 10-m wind speed. It shows that C_d gradually increases with the 10-m wind to a maximum when 10-m wind is 30 m s^{-1}, and then gradually decreases as wind further increases, before leveling off when the 10-m wind is stronger than 50 m s^{-1}. The value of C_k gradually increases to the maximum as the 10-m wind reaches 30 m s^{-1}, and then very slowly decreases as wind further increases. The ratio C_k/C_d holds closely near ~0.5 when the 10-m wind is within 30–70 m s^{-1}, which is aligned with observations (e.g., Haus et al. 2010; Bell et al. 2012). There is no coupling to an ocean or surface wave model.

d. *Analysis methods*

For vertical profiles from LES, we use horizontal averages at constant height levels. These results, as well as all SCM results, are then averaged in time using output every 1 min for the final 2 h (t = 4–6 h).

Following typical convention, TKE from LES is defined as $(1/2)(\overline{u'u'} + \overline{v'v'} + \overline{w'w'}) + e_s$, where u, v, and w are the three

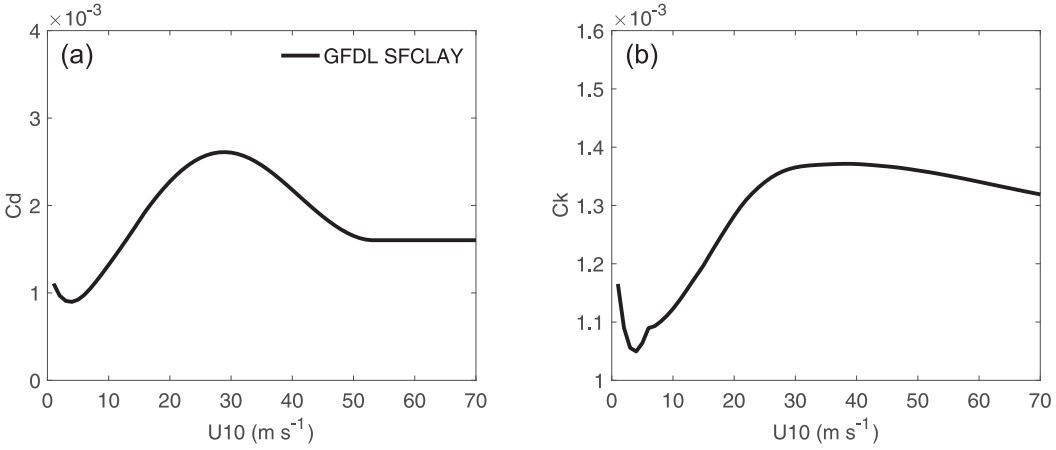

FIG. 4. The surface (a) drag coefficient and (b) enthalpy exchange coefficient under neutral conditions as a function of 10-m surface wind in the GFDL surface-layer scheme.

components of velocity, overbars denote a domain average at a specified height, primes denote perturbations from the domain average, and e_s is subgrid TKE (which comes from the subgrid model; see appendix of B17 for details). Total vertical turbulence momentum flux (τ; hereafter simply "vertical momentum flux") is defined as $[(\overline{w'u'} + \tau^t_{13})^2 + (\overline{w'v'} + \tau^t_{23})^2]^{1/2}$, where τ^t_{13} and τ^t_{23} are the subgrid turbulent momentum fluxes, which include a standard model following Deardorff (1980) and a "two-part" eddy viscosity model that acts on the mean flow (Sullivan et al. 1994; B17).

PBL depth h is defined as the height where τ becomes essentially zero. In practice, τ remains small and nonzero even above the boundary layer, so following Kosović and Curry (2000) we first find the height where τ is 5% of the surface value, and then extrapolate to where τ would be zero upon linear extrapolation from the surface. As shown in Fig. 3b, h increases rapidly in the first ~2 h of the V35 simulation, and then maintains a statistically steady value with a value of $O(1)$ km, which is similar to the typical depth of the inflow layer and the height of maximum winds in TCs (e.g., Zhang et al. 2011b).

4. LES results and verification

Figure 5 shows plan views of instantaneous horizontal wind speed at $t = 6$ h from the V45 LES output. At $z = 42.5$ m (Fig. 5a) an evident feature is the persistent "streaky" structures. These streaks are oriented approximately along the mean wind direction, with alternating low- and high-speed fluids. These characteristics are consistent with the findings in the shear-dominated boundary layer (e.g., Moeng and Sullivan 1994; Lorsolo et al. 2008), and show similarities to the boundary layer rolls documented in several studies of the hurricane boundary layer (e.g., Wurman and Winslow 1998; Morrison et al. 2005; Foster 2005). Farther aloft, at $z = 502.5$ m (Fig. 5b) the pattern appears more cellular, although elongated "steaks" are still visible, now oriented slightly more clockwise compared to low levels. It is unclear why rolls do not extend to

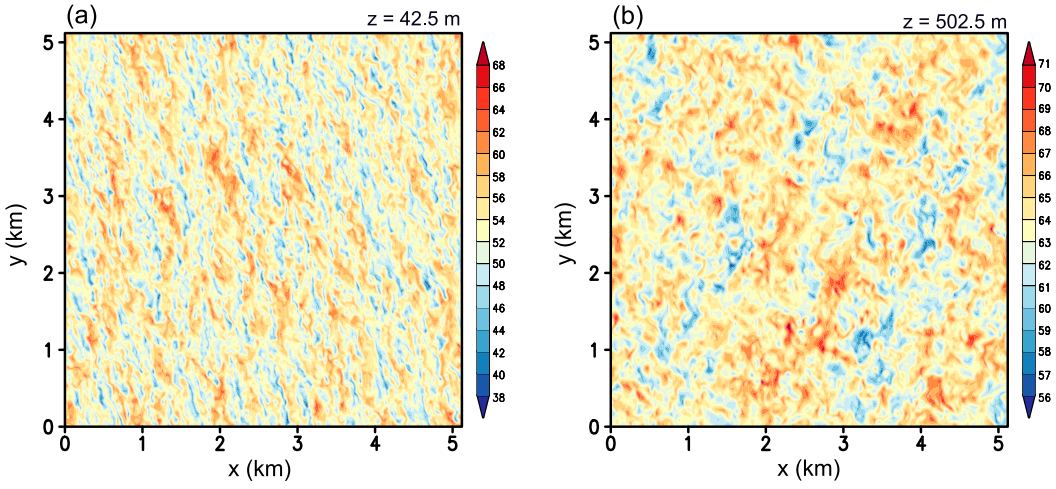

FIG. 5. Instantaneous horizontal wind speed at $t = 6$ h from the V45 simulation at (a) $z = 42.5$ m and (b) $z = 502.5$ m.

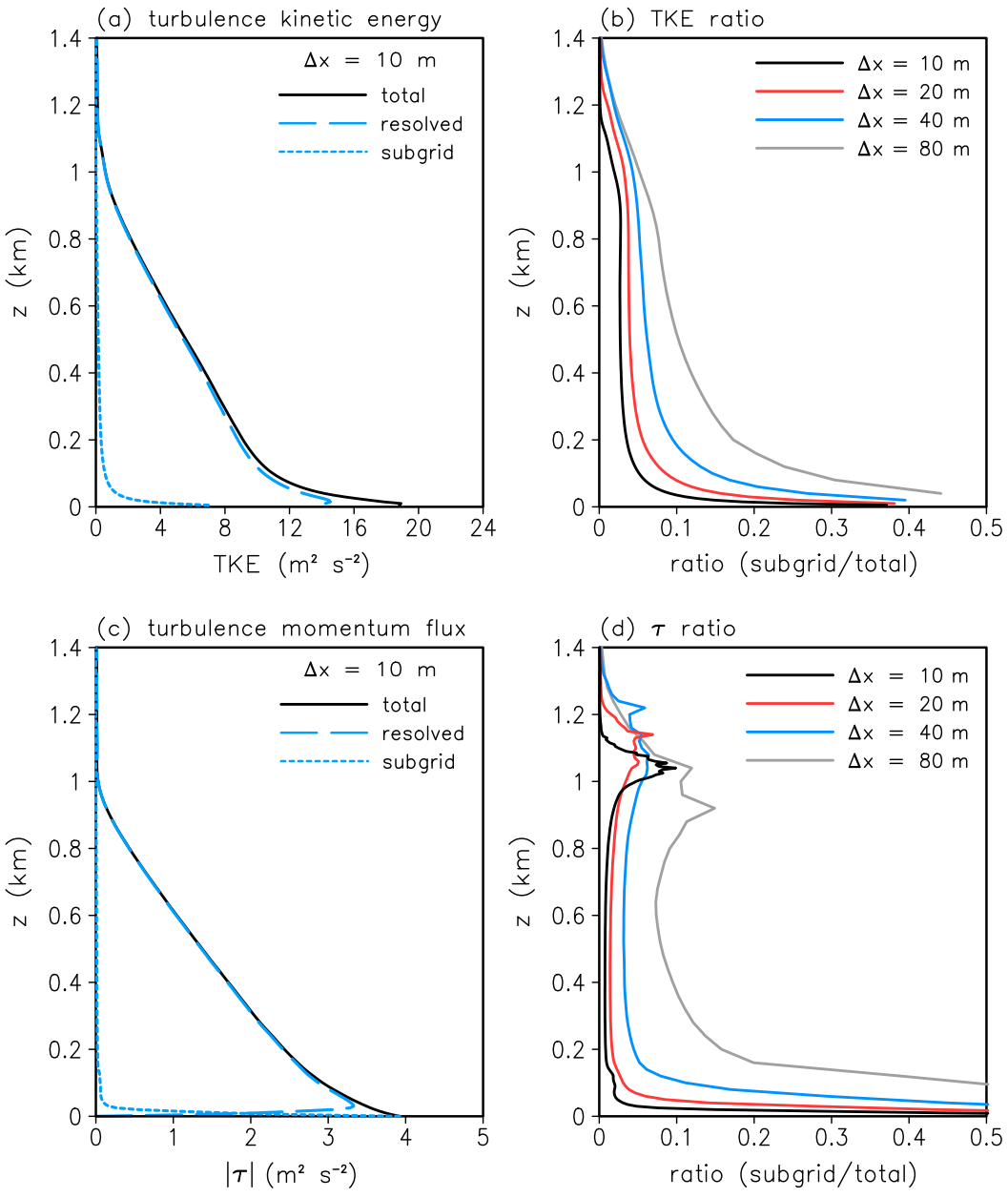

FIG. 6. Profiles of (a) turbulence kinetic energy (TKE) and (c) vertical turbulence momentum flux τ from LES with 10-m horizontal grid spacing. The solid line is the total, the long-dashed line is the resolved component, and the thin-dashed line is the subgrid component. (b),(d) The ratio of subgrid to total values is shown for four different grid spacings as indicated in the legend. All results are for V45.

the top of the boundary layer (i.e., up to ~1000 m) in these simulations, as has been observed in actual tropical cyclones (e.g., Lorsolo et al. 2008; Guimond et al. 2018).

Vertical profiles of TKE (e.g., Fig. 6a) are typical for statically neutral, shear-driven boundary layers (cf. Berg et al. 2020) in that the maximum TKE is very close to the surface, and decreases asymptotically to the top of the boundary layer. In all cases, maximum TKE is at $z \approx 10$ m ($z/h \approx 0.01$) with a peak nondimensional value of $\mathrm{TKE}/u_*^2 = 4.8$; this value is quite similar to other studies of shear-driven PBLs (e.g., Berg et al. 2020). Because observations from the surface layer in TCs are very rare, it is generally unclear how turbulence properties in the TC boundary layer compare to "ordinary" shear-driven boundary layers at much lower wind speeds. The close similarity of these results (Fig. 6a) to weaker-shear LES studies suggest that TC boundary layers are similar overall to other shear-driven boundary layers; this point is investigated further below.

Figure 6b shows the ratio of subgrid to total TKE for four simulations with varying horizontal grid spacing: $\Delta x = 10$, 20, 40, and 80 m, with vertical grid spacing (below 2 km) of 5, 10,

TABLE 3. Boundary layer height (m), averaged from 4 to 6 h, from resolution sensitivity simulations.

Δx (m)	V25	V35	V45
80	939	1100	1050
40	987	1113	1030
20	985	1068	978
10	946	996	891

20, and 40 m, respectively. As expected, the percentage of subgrid TKE is small (less than 10%) above the near-surface layer for the highest resolution simulation. For $\Delta x = 80$ m (and larger grid spacing, not shown) the subgrid TKE is an unacceptably large percentage of the total TKE (greater than 10%), demonstrating that grid spacing of $O(10)$ m is needed for well-resolved LES of the TC boundary layer in which the subgrid model plays a small role (except, of course, near the surface).

Profiles of vertical momentum flux τ (Fig. 6c) are also typical for shear-driven boundary layers, with an approximately linear decrease from the surface to the top of the boundary layer. The ratio of subgrid to total vertical momentum flux (Fig. 6d) shows that the subgrid model plays a very small role throughout most of the boundary layer; the exceptions are at the surface where vertical momentum flux is parameterized through Monin–Obukhov similarity theory, and near the top of the boundary layer where the subgrid ratio peaks at roughly 10% for all $\Delta x < 40$ m.

The average values of h from the final 2 h of all simulations are listed in Table 3, which show that h decreases slightly as Δx decreases for $\Delta x \leq 40$ m. A qualitatively similar change in h with Δx was found by Berg et al. (2020) in simulations of a sheared neutral PBL with Δx as small as 2.5 m.

To evaluate turbulence properties in these LES, we use available observational estimates of τ in hurricanes from NOAA P3 aircraft (F07; Z11; Zhang and Drennan 2012), which are plotted as dots in Figs. 7 and compared with nondimensional profiles of τ from LES. For Fig. 7a, profiles from all three cases (V25, V35, and V45) are nondimensionalized in the traditional way using the square of the surface friction velocity u_*. From the observational studies, estimates of u_* are only available from the study by F07, which are all from tropical storm–force wind speeds. Actually, all values from F07 are for 10-m wind speed less than 29 m s^{-1}, and thus are most directly applicable to the V25 simulation. Results (Fig. 7a) are comparable for all simulations when normalized by $u_*^{2\,2}$. The F07 observations in Fig. 7a tend to be larger in magnitude than the model simulations, but we suspect the observational data in this figure are biased high because of a low bias in the estimates of u_* that was identified by Andreas et al. (2012, p. 2523).

To bring more observational data into the analysis, and to remove the bias associated with the surface parameter u_*, we plot τ normalized by the square of mean wind speed U from each level. This normalization allows us to use the P3 measurements from Z11 as well as recent UAS measurements in hurricane eyewalls by C20; notably, these two studies include observations at hurricane-force wind speeds. Results (Fig. 7b) show that the three LESs do not compare quite as

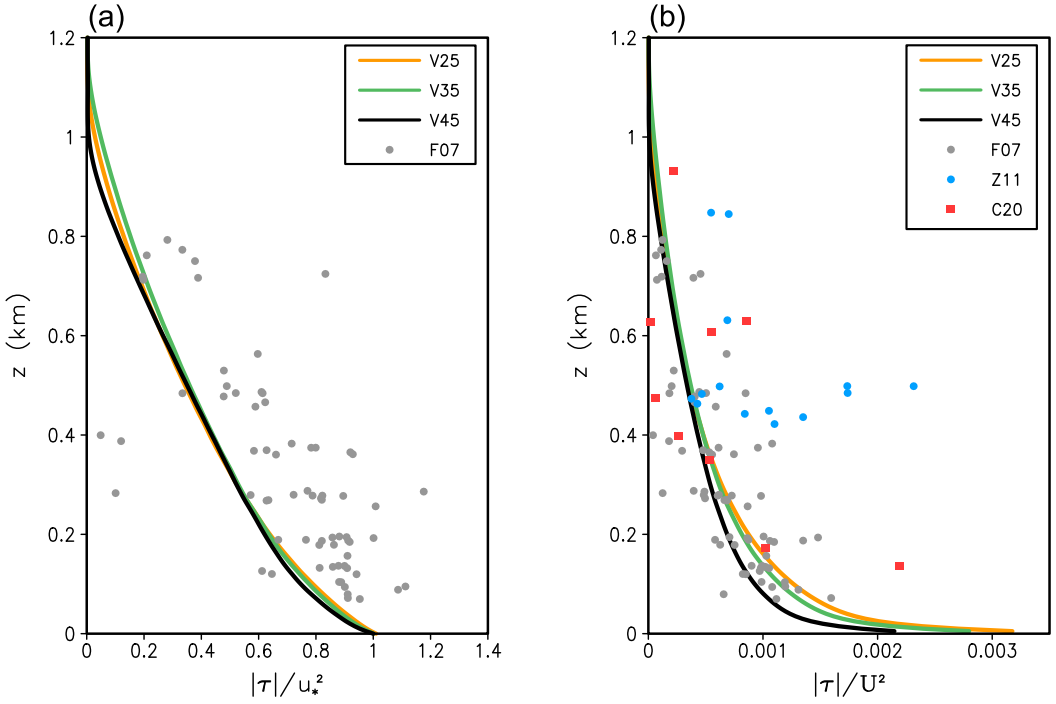

FIG. 7. Vertical profiles of total vertical turbulent momentum flux τ (m^2 s^{-2}) from LES for V25 (orange), V35 (green), and V45 (black). (a) Results nondimensionalized by u_*^2 and (b) results nondimensionalized by U^2. Dots show observations from F07 (gray), Z11 (blue), and C20 (red).

well to each other in low levels (below 400 m), but are very similar in the upper half of the boundary layer ($z > 500$ m). Most important for the present analysis is that the LES results compare well with the observations, especially for $z <$ 400 m. There are some cases where observational data points are a factor of 2 larger (e.g., at $z = 150$ m for C20, and $z =$ 500 m for Z11) which are difficult to explain here, but may be related to deep-convective processes in hurricanes that are not present in these simplified numerical simulations, or perhaps are related to ''mesovortices'' (also known as ''eyewall vorticity maxima'') which are coherent vortices of $O(1)$-km horizontal scale that are associated with localized extreme wind gusts in hurricanes (e.g., Aberson et al. 2006; Marks et al. 2008; Stern et al. 2016).

5. Comparison to an ordinary shear-driven PBL

As noted in the introduction, PBL parameterizations have generally been developed for conditions over land, or for weak winds over oceans. It is an open question whether commonly used PBL parameterizations work well in hurricane conditions, i.e., in strong winds over the oceans. As one step toward answering this question we compare the LES from this study with a standard approach for studying shear boundary layers: the Ekman-type boundary layer. We use the term ''Ekman type'' in the same sense as B17, where the pressure-gradient acceleration is computing using the geostrophic wind equation, and because we are using LES, the effective eddy viscosity is not constant (as it is in the classic Ekman spiral solution). For LES, we set the pressure gradient in the x direction to $+fV_{\text{geo}}$ (V_{geo} denotes geostrophic wind speed), and the pressure gradient in the y direction to zero, and there are no centrifugal or large-scale advective tendencies. The approach to large-scale thermodynamic tendencies is the same as before, i.e., the nudging term toward the profiles shown in Figs. 1e and 1f is retained.

Resulting mean wind profiles are presented with standard (dimensional) units as shown in Figs. 8a–c for simulations with $\Delta x = 20$ m and $\Delta z = 10$ m, where it is clear that the boundary layer depth is greater (by a factor of 2) for the Ekman-like approach as compared to the TC simulations. The much shallower boundary layer depth in TC simulations reflects the effect of TC's strong rotation on reducing boundary layer height. In fact, it takes much longer for the Ekman-like simulations to develop a steady boundary layer, so we run them for 2 days (instead of 6 h for the TC setup) and analyze the final 2 h of every simulation. The much slower development of the Ekman-type boundary layer is attributable to the longer large-eddy turnover time, which is approximated by h/u_*. The longer run time for the simulation of the Ekman-type boundary layer explains why we use a lower resolution in this section ($\Delta x = 20$ m, instead of 10 m elsewhere in this study) to reduce computational expense. Figures 6b and 6d indicate that 20-m horizontal grid spacing maintains an acceptably small ratio of parameterized subgrid processes.

In addition to the deeper boundary layer, other notable differences in Figs. 8a–c include a maximum inflow at a factor-of-10-higher height (Fig. 8a) and substantially weaker near-surface wind speeds by a factor of nearly 2 (Fig. 8c). The same differences were reported in B17, where the primary contributor to higher wind speeds was identified to be the centrifugal acceleration terms in the TC framework.

Nondimensional profiles are shown in Figs. 8d–f, using the same definition of boundary layer height h as before (see section 3e) to nondimensionalize height, and using the surface friction velocity u_* to nondimensionalize wind speeds. This analysis demonstrates that differences in the two wind profiles remain similar, i.e., for the Ekman-like simulation the height of maximum inflow remains higher above the surface, and the near-surface (for $z/h < 0.1$) wind speed remains weaker, although in the case the difference in the wind speed is much smaller (18% weaker in nondimensional wind speed, as opposed to a factor of ~2 weaker for dimensional wind speed).

Velocity variances are shown in Fig. 9 in the same manner as wind speed (Fig. 8), i.e., with dimensional profiles shown in the top row (Figs. 9a–c) and nondimensional profiles shown in the bottom row (Figs. 9d–f). As in Sullivan and Patton (2011), the subgrid variance is included by adding $2/3e_s$ to every component, essentially assuming that subgrid turbulence is isotropic. For the TC boundary layer, variances in the lower half of the boundary layer ($z < 500$ m) are substantially larger than those in an Ekman-type boundary layer, especially for the streamwise variance (Fig. 9b) which is a factor of 3 larger in the TC simulation. These results are consistent with the stronger low-level winds and wind shear noted earlier. Interestingly, when normalized by u_*^2 the variance profiles are fairly similar for all three components (Figs. 9d–f), although maximum nondimensional streamwise velocity variance is 20% larger in the TC simulation (Fig. 9e) near the surface. These results have implications for several applications, including for the design of wind turbines that are susceptible to TCs (e.g., Kapoor et al. 2020), and call for further studies into turbulence properties in TC boundary layers.

TKE profiles are shown as dashed lines in Figs. 9c and 9f. In terms of dimensional values, TKE is substantially larger (by a factor of 2–3) near the surface for the TC case. Curiously, the nondimensional TKE profiles are nearly identical (Fig. 9f).

The results in this section suggest that TC boundary layers *are* substantially different from ordinary shear-driven boundary layers when viewed with dimensional units, although when viewed with nondimensional scaling the differences are much smaller. Specifically, in dimensional terms, the TC boundary layer has a maximum inflow at a factor-of-10-shallower height, much stronger near-surface wind speed, and a factor-of-2-shallower boundary layer (with the caveat being that the thermodynamic conditions are held essentially fixed to TC-like conditions by the nudging term used herein). The TC boundary layer also achieves steady state in a factor-of-4-faster time in these simulations. In nondimensional terms, the differences are much smaller, though, and the nondimensional TKE profiles are nearly identical in the two frameworks. In terms of guidance for the development of PBL parameterizations, and analytic studies of TC boundary layers, these results show that nondimensional turbulence properties are quite similar to

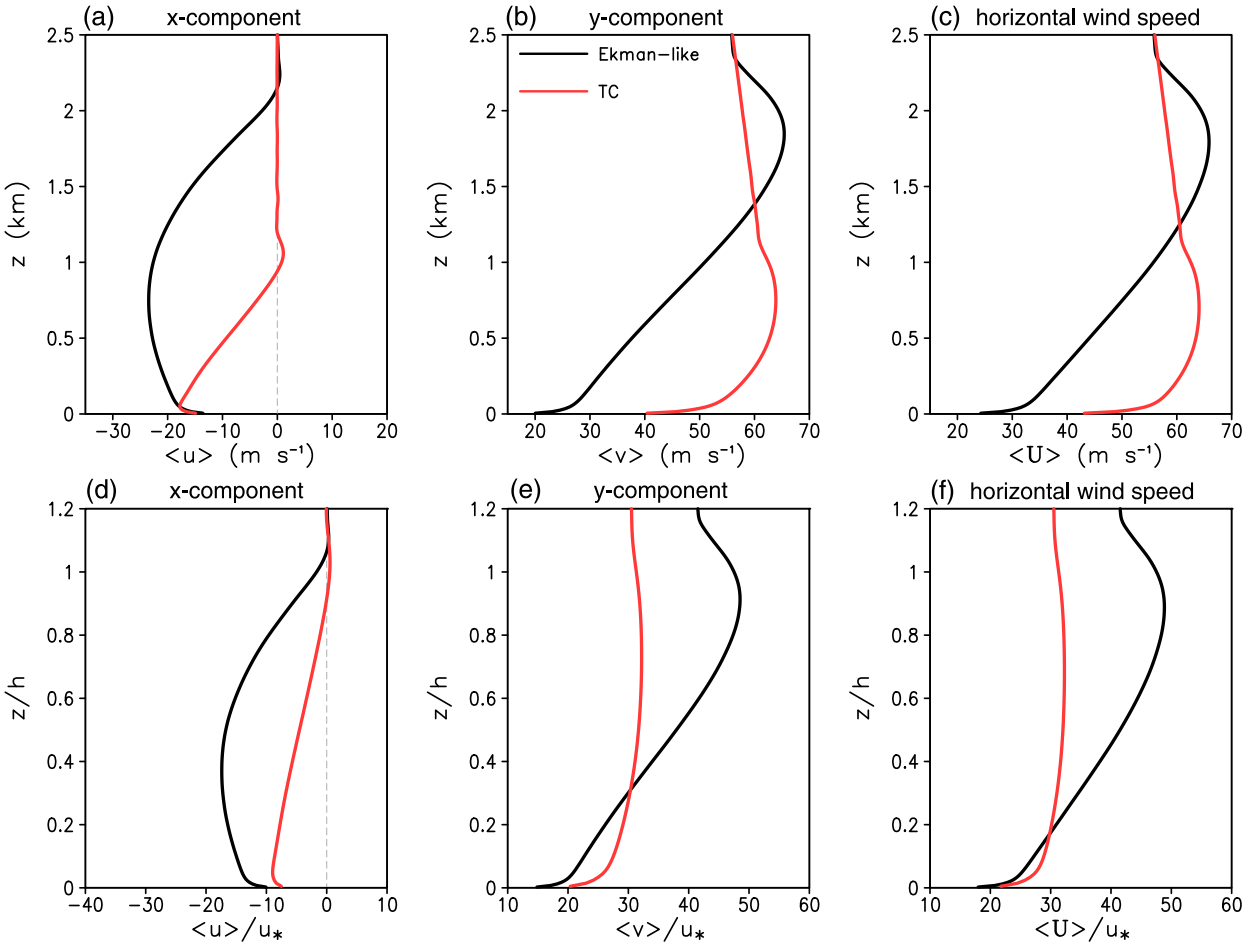

FIG. 8. Horizontal velocity components for the LES using 20-m grid spacing with the TC setup (red) and an Ekman-like setup (black). (a)–(c) Dimensional results and (d)–(f) nondimensionalized results. Columns show (a),(d) the x component of velocity (analogous to radial velocity in the TC framework), (b),(e) the y component of velocity (analogous to tangential velocity in the TC framework), and (c),(f) the total horizontal wind speed.

ordinary sheared boundary layers, despite the stark differences in mean wind profiles, and warrant a closer look at PBL parameterization performance in hurricane conditions.

6. Using LES results to evaluate PBL parameterizations

The analysis in this section highlights ways in which this modeling framework can be used to evaluate and improve PBL parameterizations in TC conditions. A key diagnostic that is useful for comparison to some PBL parameterizations is the effective vertical eddy viscosity K_{eff} which is calculated from LES and observations as

$$K_{\text{eff}} = \frac{\sqrt{\overline{w'u'}^2 + \overline{w'v'}^2}}{\sqrt{(\partial\overline{u}/\partial z)^2 + (\partial\overline{v}/\partial z)^2}} + K_m + K_w, \qquad (2)$$

where K_m denotes the standard subgrid-scale eddy viscosity (which plays a role mainly near the surface in the LES framework) and K_w denotes the near-surface eddy viscosity from the "two-part" subgrid turbulence model (B17). As expected, we find that to K_m and K_w are negligible except near the surface and entrainment layer in LESs (not shown).

Figure 10a compares K_{eff} from the LES (black line) in V25 and observed K_{eff} values determined by Zhang and Drennan (2012) (black dots) from relatively weak surface winds (18–30 m s^{-1}). As in B17, these observational data are selected when the observed wind speed at the same altitude was within 4 m s^{-1} of the domain-averaged mean wind speed from the LES. The K_{eff} profile of the LES generally passes through the central part of the dot cluster at different levels, indicating a decent agreement between the LES and observations in terms of the magnitude of K_{eff}. However, the model values tend to be larger than observations below 150 m, and smaller than observations above 150 m. This comparison provides some confidence for the fidelity of the LES framework; however, measurements of effective eddy viscosity are scarce at higher wind speeds, which would be needed for further confidence in high-wind TC LES modeling. We also note that the effective eddy viscosity in LES is larger in magnitude for higher wind speeds (i.e., the maximum value increases from 40 m^2 s^{-1} for V25 to 60 m^2 s^{-1} for V45) as expected for the associated higher wind shear.

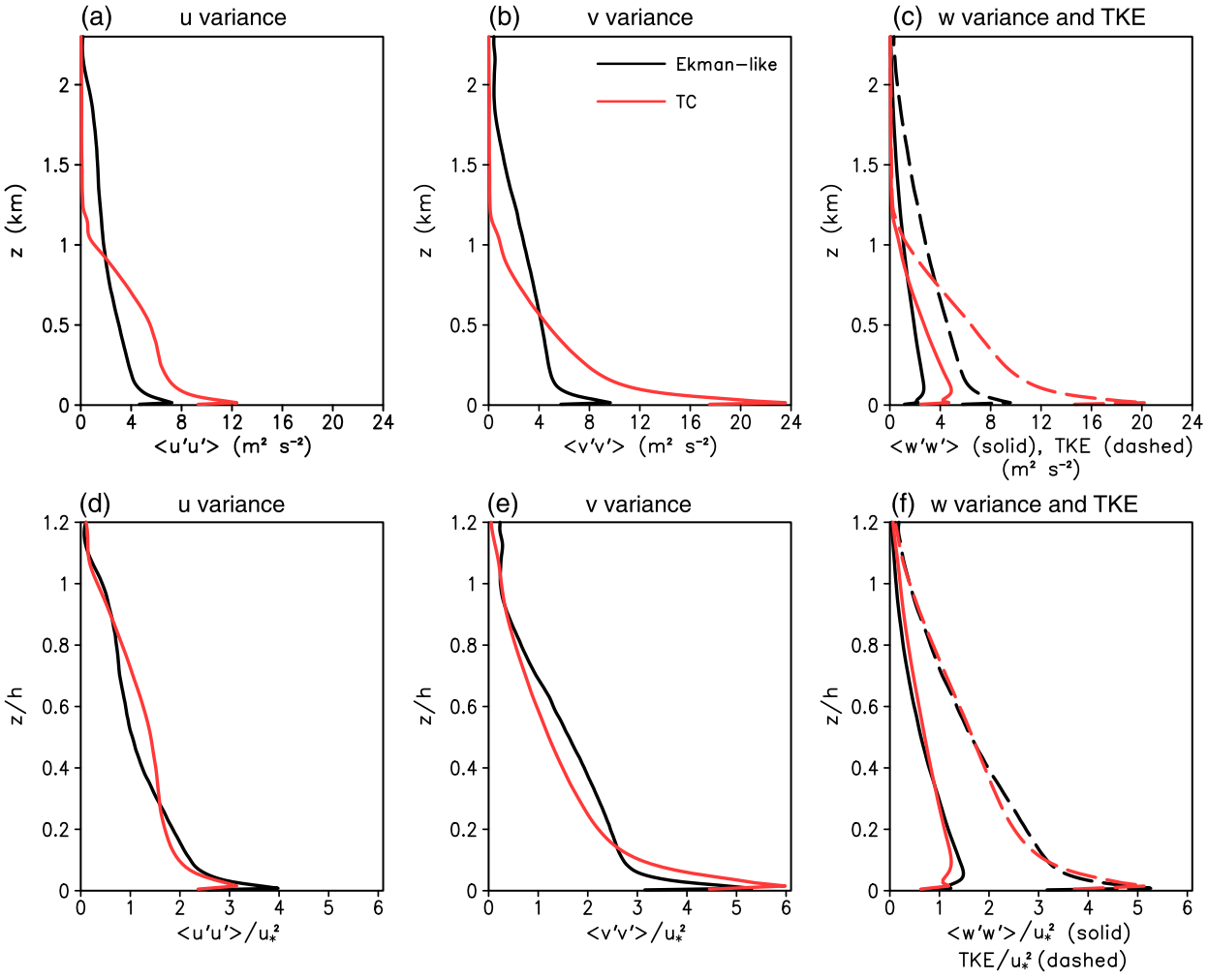

FIG. 9. Turbulence velocity variances for LES using 20-m grid spacing with the TC setup (red) and an Ekman-like setup (black). (a)–(c) Dimensional results and (d)–(f) nondimensionalized results. Columns show (a),(d) the variance for the x component of velocity (analogous to radial velocity in the TC framework), (b),(e) the variance for the y component of velocity (analogous to tangential velocity in the TC framework), and (c),(f) the vertical velocity variance (solid lines) and the TKE (dashed lines).

Of particular note for all simulations is the height of maximum K_{eff}, which is ≈200 m in all simulations, or approximately $h/5$. This level is important to determine because it suggests a level at which to focus future observational analysis, e.g., using UASs to collect data in hazardous conditions (e.g., C20). Another reason this height is relevant is because of so-called K-profile parameterization (KPP) approaches for PBL schemes used in weather prediction models (e.g., NOAA's operational HWRF Model uses a KPP scheme). Thus, an evaluation of this approach is highly relevant to modeling the TC boundary layer. KPP schemes typically use the parametric profile

$$K = \kappa u_* z \left(1 - \frac{z}{h}\right)^2, \tag{3}$$

where $\kappa = 0.4$ is the von Kármán constant, and h is PBL depth (typically determined in these PBL schemes by a critical value of bulk Richardson number). As noted by O'Brien (1970) and Kepert (2012), the profile in (3) has a maximum value at $z = h/3$, which is approximately a factor of 2 higher than the height of maximum K_{eff} in the LESs (Fig. 10). To illustrate the difference between the model-derived profiles of K_{eff} and (3), we use the model-produced values of u_* and h (using the method described in section 3e) and plot the results as long-dashed lines in Fig. 10. The profile (3) is clearly different compared to LES, and suggests that using (3) in TC boundary layers is inherently flawed (assuming, of course, that the LES results are an accurate representation of nature). To reduce the level of maximum K, as well as the maximum amplitude of K, one could simply change the exponent in the parametric profile, i.e.,

$$K = \kappa u_* z \left(1 - \frac{z}{h}\right)^4, \tag{4}$$

which has maximum K at $z = h/5$ (roughly the same as LES results). This profile is shown using short-dashed lines in Fig. 10,

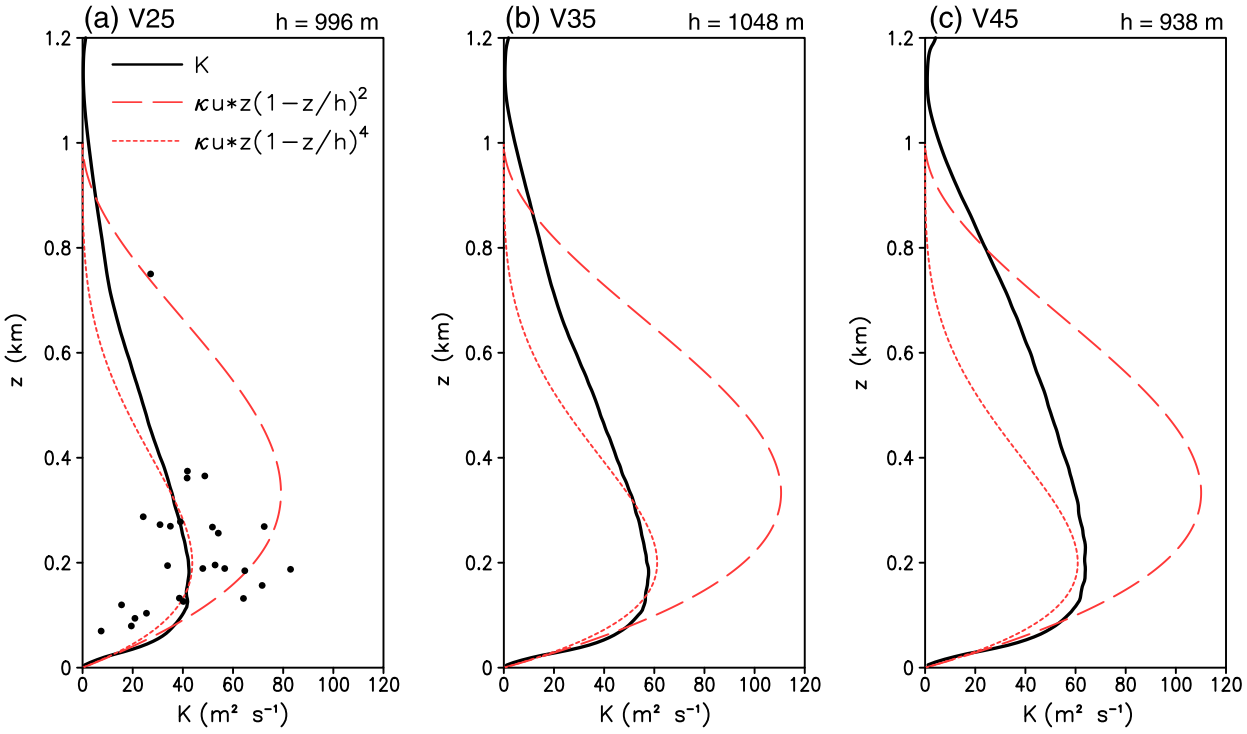

FIG. 10. Vertical profiles of effective eddy diffusivity K (black lines) for (a) V25, (b) V35, and (c) V45. Black dots in (a) denote observational estimates from Zhang and Drennan (2012). The dashed and dotted red lines indicate analytic profiles as indicated by the legend in (a).

which are a better (although clearly not perfect) match to the LES results. These results suggest that KPP schemes should not be used for hurricane boundary layers; further results, using (3) and (4) in single-column model simulations, will be reported in a forthcoming article. We reiterate that additional measurements of vertical momentum fluxes and vertical wind profiles (which are needed to calculate $K_{\rm eff}$) are necessary at more heights and higher wind speeds than were determined by Zhang and Drennan (2012).

Another insightful variable that can be calculated from LES output, and can be used in PBL parameterizations, is the effective turbulence length scale, calculated as

$$l_{\rm eff} = \left(K_{\rm eff} \Big/ \sqrt{(\partial\overline{u}/\partial z)^2 + (\partial\overline{v}/\partial z)^2} \right)^{1/2}, \qquad (5)$$

which is plotted in Fig. 11 for all three TC LESs. The profiles (solid colored lines in Fig. 11) are very similar in these three cases, with a maximum value of approximately 40 m at z = 250 m (or roughly $z = h/4$). The LES-determined values of $l_{\rm eff}$ are similar to the observational estimates from Zhang and Drennan (2012) (dots in Fig. 11a), at least in the sense that there is a linear increase from the surface to about 200 m, and roughly constant values with an average of order 40 m above. However, the scatter in the observations is large, and the LES values are consistently larger than the observational estimates below 200 m.

Estimates of $l_{\rm eff}$ are important for the first-order PBL model that is used by default for hurricane simulations in CM1. Specifically, the BR09 PBL scheme, with modifications by B17, uses a mixing-length formulation from the relation (Mason and Thomson 1992)

$$\frac{1}{l^2} = \frac{1}{(\kappa z)^2} + \frac{1}{l_\infty^2}, \qquad (6)$$

where l_∞ is a specified "asymptotic" length scale in CM1. This formulation with l_∞ = 40 m is shown as a short-dashed line in Fig. 11b; comparison with $l_{\rm eff}$ from LES results is reasonable for $z < 400$ m, although it underestimates LES results by about 10% at z = 300 m. Comparison above 500 m is not as good, since clearly a constant value in the upper half of the PBL is a poor assumption (according to LES results). The effects of static stability likely need to be considered in a more accurate formulation for l. Nevertheless, the formulation in (6) is clearly a better match to LES results than the often-used formulation (usually attributed to Blackadar 1962)

$$\frac{1}{l} = \frac{1}{\kappa z} + \frac{1}{l_\infty}, \qquad (7)$$

which is plotted as a dotted line in Fig. 11b assuming l_∞ = 40 m. Clearly, (6) is a better match to LES results than (7), which supports the use of (6) in the BR09 PBL scheme.

The default value for l_∞ in CM1 is 75 m, which is nearly a factor of 2 larger than the LES results and observations (Fig. 11a). To see whether a smaller value matching LES and observations can produce more realistic results, we use the LES as a benchmark and run SCM simulations (see section 3d for details) using the BR09 PBL scheme. Values of eddy diffusivity K from the BR09

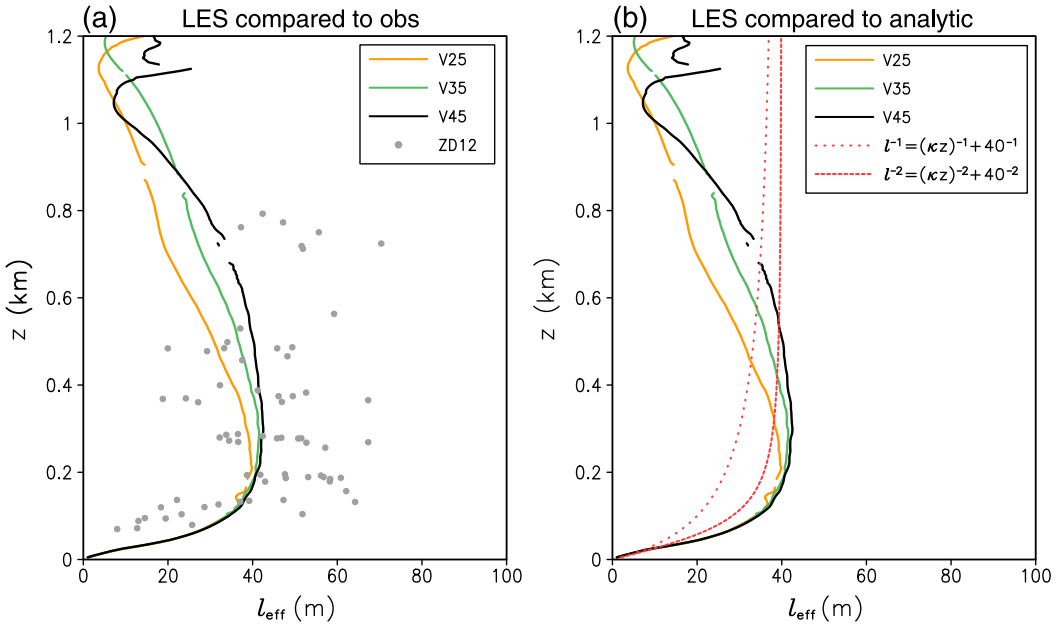

FIG. 11. (a) Vertical profiles of the effective mixing length l_{eff} from LES for V25 (orange), V35 (green), and V45 (black). Dots in (a) are observational estimates of l_{eff} from Zhang and Drennan (2012). (b) Dashed and dotted red lines denote analytic profiles using $l_\infty = 40$ m as indicated in the legend.

scheme are shown in Figs. 12a–c. Results using $l_\infty = 75$ m are shown in blue, which are clearly larger (by a factor of 2) than K_{eff} from LES. Results using $l_\infty = 40$ m are shown in red, which are a much closer match to the LES results. Profiles of the radial component of velocity (u) in Figs. 11d–f show a clear advantage to $l_\infty = 40$ m, both in terms of matching the minimum value of u near the surface and reproducing the inflow-layer depth (i.e., height where u first goes to zero). Similarly, for the tangential component of velocity (v) in Figs. 11g–i, there is a better match to LES results for $l_\infty = 40$ m. Surface wind speed and boundary layer depth are also a better match to LES results with the lower value of l_∞ (Fig. 3). These results demonstrate the value of this LES framework in evaluating PBL schemes in TC conditions where observations are presently scarce or nonexistent.

7. Conclusions

Understanding of turbulence characteristics in the TC boundary layer remains challenging, mostly due to insufficient observations. Additionally, planetary boundary layer (PBL) schemes in numerical models are mostly designed for nonhurricane conditions, and uncertainties of applying these PBL schemes to hurricane conditions remains poorly understood. To fill in this gap, this study presented and evaluated a modeling framework specifically for the TC boundary layer that can be used for a small-domain [O(5)-km] large-eddy simulations (LES) (which do not require PBL parameterization) and also single-column modeling (SCM) using different PBL schemes. Building upon a simple technique of simulating boundary layer winds of TCs that includes several key input parameters to represent the TC structure (B17), this framework includes a one-dimensional nudging tendency to "anchor" the moisture and temperature profiles from actual major hurricanes during the simulations, which allows us to bypass the complex settings for radiation, microphysics, and other physical processes. Simulations with this framework do not produce the excessive growth of the boundary layer height in high-wind conditions reported in B17, which did not apply thermodynamic nudging. The reference thermodynamic profiles at different high-wind conditions are derived based on a composite analysis of dropsonde observations for category 4–5 hurricanes over 1999–2010.

With this framework, steady conditions develop in a short time (~2.5 h) in both LES and SCM. Results from LESs with different horizontal grid spacing show that turbulence kinetic energy (TKE) and vertical momentum flux are mostly resolved and the subgrid-scale terms are comparably negligible only when the horizontal grid spacing is O(10) m. Profiles of vertical momentum flux, effective eddy viscosity, and turbulence length scale from LES agree well with observational values in hurricanes of various intensity. This comparison also highlights that future observations based on advanced platforms [e.g., small unmanned aircraft system (sUAS)] need to focus on the surface layer (<100 m), where observations are very scare, and the level of ~200 m, where both effective eddy viscosity and turbulence length scale are maximized according to LES.

Comparison of LES results with thermodynamic nudging but using traditional "Ekman-like" tendency terms under geostrophic conditions also show that vertical profiles of TKE and velocity variances in the TC boundary layer are similar to previous studies for "ordinary" neutral, shear-driven boundary layers. Comparison of these results to the TC framework indicates that the TC boundary layer is much shallower, develops to steady conditions much faster, and has stronger near-surface wind speed and velocity variances. These differences can be attributed to the effect of

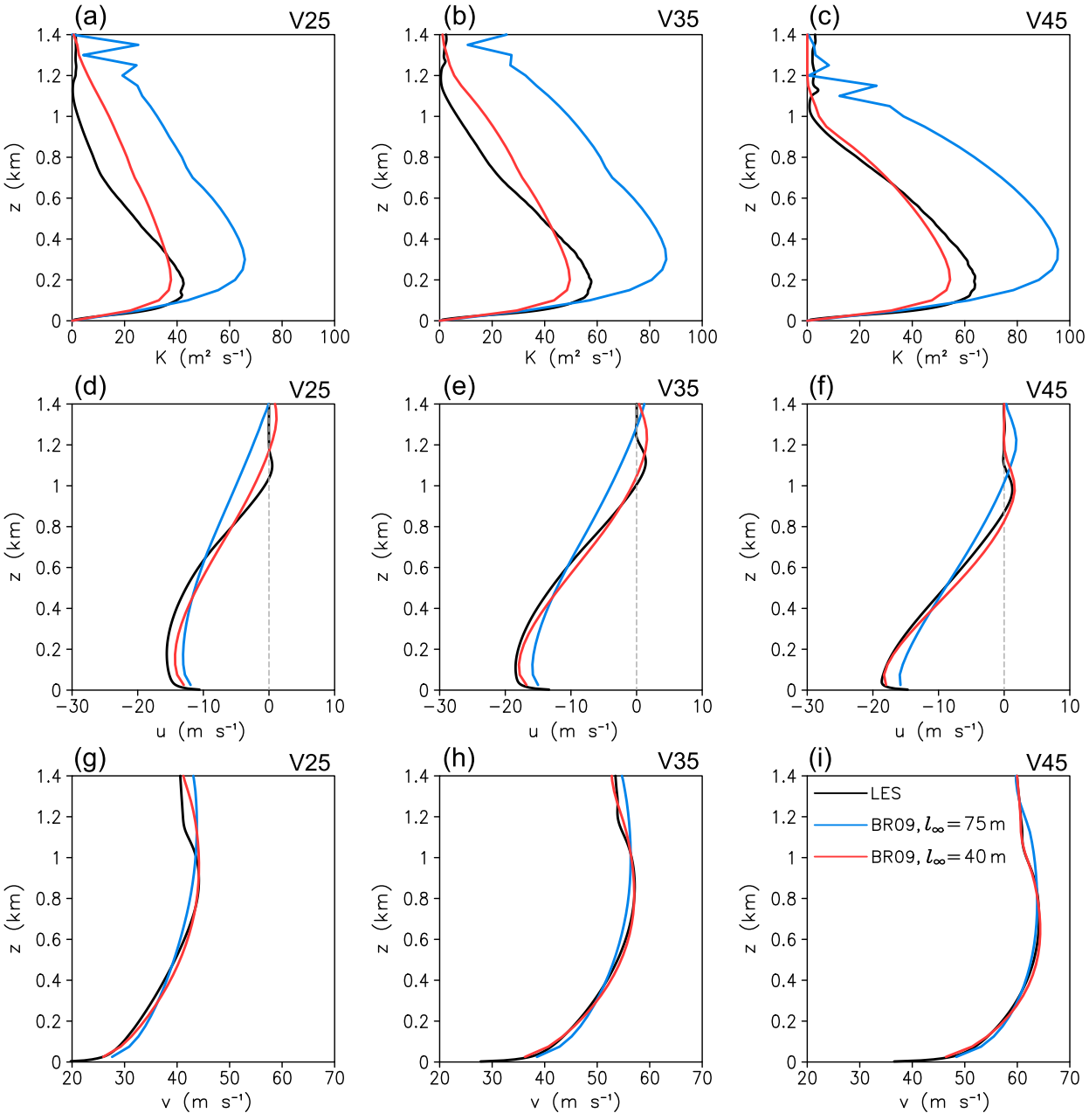

FIG. 12. Single-column modeling results using the BR09 PBL (red and blue lines) and LES results (black lines) for (left) V25, (center) V35, and (right) V45. Blue line shows results with $l_\infty = 75$ m, and red line shows results with $l_\infty = 40$ m. (a)–(c) Eddy viscosity K ($m^2 s^{-1}$), (d)–(f) radial wind u ($m s^{-1}$), and (g)–(i) tangential wind v ($m s^{-1}$). The gray dashed line in (d)–(f) marks $u = 0 m s^{-1}$.

the TC's rotation and the associated centrifugal acceleration. However, when plotted nondimensionally, the profiles of velocity variance are quite similar, and the TKE profiles are practically identical, for the Ekman-like and TC conditions.

We further demonstrated that the LES data with this framework can be used to evaluate a PBL parameterization used for hurricane simulations. In this Louis-type PBL scheme (BR09) the vertical mixing length above the surface layer is predominantly determined by a fixed asymptotic length scale l_∞. Compared to the LES results, the default setting of BR09 with $l_\infty = 75$ m produces an excessively deep inflow layer with weaker inflow strength due to excessive vertical mixing. By setting $l_\infty = 40$ m, a value more consistent with LES results, the simulated tangential and radial wind profiles from BR09 are more similar to the LES counterparts. Another important finding to note is the formulation for turbulence length scale near the surface following Mason and Thomson (1992) is a better match to both observations and LES results than the often-used Blackadar formulation (Blackadar 1962). For the K-profile parameterization (KPP), LES results suggest that the exponent in the parametric profile needs to be increased for

hurricane conditions such that the maximum eddy viscosity is reduced in magnitude and located closer to the surface.

As a concluding note, it should be noted that in the spirit of a "simple" approach, this framework does not account for complex mesoscale processes and rapidly evolving conditions (e.g., rapid intensification or weakening), and cannot address all types of TC boundary layers. There are clearly advantages to studying PBL schemes in more realistic but complex conditions, such as in a long-duration "full physics" modeling system with real-data initial conditions, which this framework cannot reproduce. However, the merits of this approach include the ability to use high resolution (e.g., 10-m grid spacing) and modest supercomputing resources, and the ability to compare different underlying assumptions in PBL schemes under controlled and known hurricane conditions. In a forthcoming paper, we will document a detailed evaluation of different types of PBL schemes and the suggested revisions to these PBL schemes in hurricane conditions using this modeling framework. Examinations of the effects of the revised PBL schemes on the three-dimensional simulations of TCs are also underway.

Acknowledgments. We would like to acknowledge high-performance computing support from Cheyenne (doi:10.5065/D6RX99HX) provided by NCAR's Computational and Information Systems Laboratory, sponsored by the National Science Foundation. The authors benefited from the communication with Prof. Robert Fovell and Dr. Evan Kalina regarding the discussions of PBL schemes. We want to acknowledge Drs. Gopal Sundararaman, Andy Hazelton, and three anonymous reviewers for their helpful suggestions to improve this manuscript. The first author, Xiaomin Chen, was supported by the NRC Research Associateship award and Award NA21OAR4320190 to the Northern Gulf Institute at Mississippi State University from NOAA's Office of Oceanic and Atmospheric Research, U.S. Department of Commerce. George Bryan is supported by the National Center for Atmospheric Research, which is a major facility sponsored by the National Science Foundation under Cooperative Agreement 1852977, and by Office of Naval Research Grant N00014-20-1-2071. Jun A. Zhang was supported by NSF Grant AGS-1822128 and ONR Grant N00014-20-1-2071.

REFERENCES

Aberson, S. D., M. T. Montgomery, M. Bell, and M. Black, 2006: Hurricane Isabel (2003): New insights into the physics of intense storms. Part II: Extreme localized wind. *Bull. Amer. Meteor. Soc.*, **87**, 1349–1354, https://doi.org/10.1175/BAMS-87-10-1349.

Andreas, E. L., L. Mahrt, and D. Vickers, 2012: A new drag relation for aerodynamically rough flow over the ocean. *J. Atmos. Sci.*, **69**, 2520–2537, https://doi.org/10.1175/JAS-D-11-0312.1.

Bell, M. M., M. T. Montgomery, and K. A. Emanuel, 2012: Air–sea enthalpy and momentum exchange at major hurricane wind speeds observed during CBLAST. *J. Atmos. Sci.*, **69**, 3197–3222, https://doi.org/10.1175/JAS-D-11-0276.1.

Berg, J., E. G. Patton, and P. P. Sullivan, 2020: Large-eddy simulation of conditionally neutral boundary layers: A mesh resolution sensitivity study. *J. Atmos. Sci.*, **77**, 1969–1991, https://doi.org/10.1175/JAS-D-19-0252.1.

Blackadar, A. K., 1962: The vertical distribution of wind and turbulent exchange in a neutral atmosphere. *J. Geophys. Res.*, **67**, 3095–3102, https://doi.org/10.1029/JZ067i008p03095.

Braun, S. A., and W.-K. Tao, 2000: Sensitivity of high-resolution simulations of Hurricane Bob (1991) to planetary boundary layer parameterizations. *Mon. Wea. Rev.*, **128**, 3941–3961, https://doi.org/10.1175/1520-0493(2000)129<3941:SOHRSO>2.0.CO;2.

Bryan, G. H., and J. M. Fritsch, 2002: A benchmark simulation for moist nonhydrostatic numerical models. *Mon. Wea. Rev.*, **130**, 2917–2928, https://doi.org/10.1175/1520-0493(2002)130<2917:ABSFMN>2.0.CO;2.

——, and R. Rotunno, 2009: The maximum intensity of tropical cyclones in axisymmetric numerical model simulations. *Mon. Wea. Rev.*, **137**, 1770–1789, https://doi.org/10.1175/2008MWR2709.1.

——, R. P. Worsnop, J. K. Lundquist, and J. A. Zhang, 2017: A simple method for simulating wind profiles in the boundary layer of tropical cyclones. *Bound.-Layer Meteor.*, **162**, 475–502, https://doi.org/10.1007/s10546-016-0207-0.

Bu, Y. P., R. G. Fovell, and K. L. Corbosiero, 2017: The influences of boundary layer mixing and cloud-radiative forcing on tropical cyclone size. *J. Atmos. Sci.*, **74**, 1273–1292, https://doi.org/10.1175/JAS-D-16-0231.1.

Chen, X., K. Zhao, W.-C. Lee, B. Jong-Dao Jou, M. Xue, and P. R. Harasti, 2013: The improvement to the environmental wind and tropical cyclone circulation retrievals with the modified GBVTD (MGBVTD) technique. *J. Appl. Meteor. Climatol.*, **52**, 2493–2508, https://doi.org/10.1175/JAMC-D-13-031.1.

Cione, J. J., 2015: The relative roles of the ocean and atmosphere as revealed by buoy air–sea observations in hurricanes. *Mon. Wea. Rev.*, **143**, 904–913, https://doi.org/10.1175/MWR-D-13-00380.1.

——, P. G. Black, and S. H. Houston, 2000: Surface observations in the hurricane environment. *Mon. Wea. Rev.*, **128**, 1550–1561, https://doi.org/10.1175/1520-0493(2000)128<1550:SOITHE>2.0.CO;2.

——, and Coauthors, 2020: Eye of the storm: Observing hurricanes with a small unmanned aircraft system. *Bull. Amer. Meteor. Soc.*, **101**, E186–E205, https://doi.org/10.1175/BAMS-D-19-0169.1.

Deardorff, J. W., 1980: Stratocumulus-capped mixed layers derived from a three-dimensional model. *Bound.-Layer Meteor.*, **18**, 495–527, https://doi.org/10.1007/BF00119502.

Eliassen, A., 1971: On the Ekman layer in a circular vortex. *J. Meteor. Soc. Japan*, **49A**, 784–789, https://doi.org/10.2151/jmsj1965.49A.0_784.

Foster, R. C., 2005: Why rolls are prevalent in the hurricane boundary layer. *J. Atmos. Sci.*, **62**, 2647–2661, https://doi.org/10.1175/JAS3475.1.

——, 2009: Boundary-layer similarity under an axisymmetric, gradient wind vortex. *Bound.-Layer Meteor.*, **131**, 321–344, https://doi.org/10.1007/s10546-009-9379-1.

French, J. R., W. M. Drennan, J. A. Zhang, and P. G. Black, 2007: Turbulent fluxes in the hurricane boundary layer. Part I: Momentum flux. *J. Atmos. Sci.*, **64**, 1089–1102, https://doi.org/10.1175/JAS3887.1.

Green, B. W., and F. Zhang, 2015: Idealized large-eddy simulations of a tropical cyclone–like boundary layer. *J. Atmos. Sci.*, **72**, 1743–1764, https://doi.org/10.1175/JAS-D-14-0244.1.

Guimond, S. R., J. A. Zhang, J. W. Sapp, and S. J. Frasier, 2018: Coherent turbulence in the boundary layer of Hurricane Rita (2005) during an eyewall replacement cycle. *J. Atmos. Sci.*, **75**, 3071–3093, https://doi.org/10.1175/JAS-D-17-0347.1.

Haus, B. K., D. Jeong, M. A. Donelan, J. A. Zhang, and I. Savelyev, 2010: Relative rates of sea-air heat transfer and frictional drag in very high winds. *Geophys. Res. Lett.*, **37**, L07802, https://doi.org/10.1029/2009GL042206.

Hock, T. F., and J. L. Franklin, 1999: The NCAR GPS dropwindsonde. *Bull. Amer. Meteor. Soc.*, **80**, 407–420, https://doi.org/10.1175/1520-0477(1999)080<0407:TNGD>2.0.CO;2.

Hughes, L. A., 1952: On the low-level structure of tropical storms. *J. Meteor.*, **9**, 422–428, https://doi.org/10.1175/1520-0469(1952)009<0422:OTLLSO>2.0.CO;2.

Kapoor, A., and Coauthors, 2020: Hurricane eyewall winds and structural response of wind turbines. *Wind Energ. Sci.*, **5**, 89–104, https://doi.org/10.5194/wes-5-89-2020.

Kepert, J., 2001: The dynamics of boundary layer jets within the tropical cyclone core. Part I: Linear theory. *J. Atmos. Sci.*, **58**, 2469–2484, https://doi.org/10.1175/1520-0469(2001)058<2469:TDOBLJ>2.0.CO;2.

——, 2012: Choosing a boundary layer parameterization for tropical cyclone modeling. *Mon. Wea. Rev.*, **140**, 1427–1445, https://doi.org/10.1175/MWR-D-11-00217.1.

Kosović, B., and J. A. Curry, 2000: A large eddy simulation study of a quasi-steady, stably stratified atmospheric boundary layer. *J. Atmos. Sci.*, **57**, 1052–1068, https://doi.org/10.1175/1520-0469(2000)057<1052:ALESSO>2.0.CO;2.

Kurihara, Y., and R. E. Tuleya, 1974: Structure of a tropical cyclone developed in a three-dimensional numerical simulation model. *J. Atmos. Sci.*, **31**, 893–919, https://doi.org/10.1175/1520-0469(1974)031<0893:SOATCD>2.0.CO;2.

Li, X., and Z. Pu, 2021: Vertical eddy diffusivity parameterization based on a large-eddy simulation and its impact on prediction of hurricane landfall. *Geophys. Res. Lett.*, **48,** e2020GL090703, https://doi.org/10.1029/2020GL090703.

Lorsolo, S., J. L. Schroeder, P. Dodge, and F. Marks Jr., 2008: An observational study of hurricane boundary layer small-scale coherent structures. *Mon. Wea. Rev.*, **136**, 2871–2893, https://doi.org/10.1175/2008MWR2273.1.

Mallen, K. J., M. T. Montgomery, and B. Wang, 2005: Reexamining the near-core radial structure of the tropical cyclone primary circulation: Implications for vortex resiliency. *J. Atmos. Sci.*, **62**, 408–425,https://doi.org/10.1175/JAS-3377.1.

Marks, F. D., P. G. Black, M. T. Montgomery, and R. W. Burpee, 2008: Structure of the eye and eyewall of Hurricane Hugo (1989). *Mon. Wea. Rev.*, **136**, 1237–1259, https://doi.org/10.1175/2007MWR2073.1.

Mason, P. J., and D. J. Thomson, 1992: Stochastic backscatter in large-eddy simulations of boundary layers. *J. Fluid Mech.*, **242**, 51–78, https://doi.org/10.1017/S0022112092002271.

Moeng, C.-H., and P. P. Sullivan, 1994: A comparison of shear- and buoyancy-driven planetary boundary layer flows. *J. Atmos. Sci.*, **51**, 999–1022, https://doi.org/10.1175/1520-0469(1994)051<0999:ACOSAB>2.0.CO;2.

Morrison, I., S. Businger, F. Marks, P. Dodge, and J. A. Businger, 2005: An observational case for the prevalence of roll vortices in the hurricane boundary layer. *J. Atmos. Sci.*, **62**, 2662–2673, https://doi.org/10.1175/JAS3508.1.

Nolan, D. S., D. P. Stern, and J. A. Zhang, 2009: Evaluation of planetary boundary layer parameterizations in tropical cyclones by comparison of in situ observations and high-resolution simulations of Hurricane Isabel (2003). Part II: Inner-core boundary layer and eyewall structure. *Mon. Wea. Rev.*, **137**, 3675–3698, https://doi.org/10.1175/2009MWR2786.1.

O'Brien, J. J., 1970: A note on the vertical structure of the eddy exchange coefficient in the planetary boundary layer. *J. Atmos. Sci.*, **27**, 1213–1215, https://doi.org/10.1175/1520-0469(1970)027<1213:ANOTVS>2.0.CO;2.

Rotunno, R., Y. Chen, W. Wang, C. Davis, J. Dudhia, and G. J. Holland, 2009: Large-eddy simulation of an idealized tropical cyclone. *Bull. Amer. Meteor. Soc.*, **90**, 1783–1788, https://doi.org/10.1175/2009BAMS2884.1.

Smith, R. K., and G. L. Thomsen, 2010: Dependence of tropical-cyclone intensification on the boundary-layer representation in a numerical model. *Quart. J. Roy. Meteor. Soc.*, **136**, 1671–1685, https://doi.org/10.1002/qj.687.

——, and M. T. Montgomery, 2015: Toward clarity on understanding tropical cyclone intensification. *J. Atmos. Sci.*, **72**, 3020–3031, https://doi.org/10.1175/JAS-D-15-0017.1.

Stern, D. P., and G. H. Bryan, 2018: Using simulated dropsondes to understand extreme updrafts and wind speeds in tropical cyclones. *Mon. Wea. Rev.*, **146**, 3901–3925, https://doi.org/10.1175/MWR-D-18-0041.1.

——, ——, and S. D. Aberson, 2016: Extreme low-level updrafts and wind speeds measured by dropsondes in tropical cyclones. *Mon. Wea. Rev.*, **144**, 2177–2204, https://doi.org/10.1175/MWR-D-15-0313.1.

Sullivan, P. P., and E. G. Patton, 2011: The effect of mesh resolution on convective boundary layer statistics and structures generated by large-eddy simulation. *J. Atmos. Sci.*, **68**, 2395–2415, https://doi.org/10.1175/JAS-D-10-05010.1.

——, J. C. McWilliams, and C.-H. Moeng, 1994: A subgrid-scale model for large-eddy simulation of planetary boundary-layer flows. *Bound.-Layer Meteor.*, **71**, 247–276, https://doi.org/10.1007/BF00713741.

Worsnop, R. P., G. H. Bryan, J. K. Lundquist, and J. A. Zhang, 2017: Using large-eddy simulations to define spectral and coherence characteristics of the hurricane boundary layer for wind-energy applications. *Bound.-Layer Meteor.*, **165**, 55–86, https://doi.org/10.1007/s10546-017-0266-x.

Wu, L., Q. Liu, and Y. Li, 2018: Prevalence of tornado-scale vortices in the tropical cyclone eyewall. *Proc. Natl. Acad. Sci. USA*, **115**, 8307–8310, https://doi.org/10.1073/pnas.1807217115.

Wurman, J., and J. Winslow, 1998: Intense sub-kilometer-scale boundary layer rolls observed in Hurricane Fran. *Science*, **280**, 555–557, https://doi.org/10.1126/science.280.5363.555.

Zhang, F., and Z. Pu, 2017: Effects of vertical eddy diffusivity parameterization on the evolution of landfalling hurricanes. *J. Atmos. Sci.*, **74**, 1879–1905, https://doi.org/10.1175/JAS-D-16-0214.1.

Zhang, J. A., and W. M. Drennan, 2012: An observational study of vertical eddy diffusivity in the hurricane boundary layer. *J. Atmos. Sci.*, **69**, 3223–3236, https://doi.org/10.1175/JAS-D-11-0348.1.

——, F. D. Marks, M. T. Montgomery, and S. Lorsolo, 2011a: An estimation of turbulent characteristics in the low-level region of intense Hurricanes Allen (1980) and Hugo (1989). *Mon. Wea. Rev.*, **139**, 1447–1462, https://doi.org/10.1175/2010MWR3435.1.

——, R. F. Rogers, D. S. Nolan, and F. D. Marks, 2011b: On the characteristic height scales of the hurricane boundary layer. *Mon. Wea. Rev.*, **139**, 2523–2535, https://doi.org/10.1175/MWR-D-10-05017.1.

——, ——, P. D. Reasor, E. W. Uhlhorn, and F. D. Marks, 2013: Asymmetric hurricane boundary layer structure from dropsonde composites in relation to the environmental vertical wind shear. *Mon. Wea. Rev.*, **141**, 3968–3984, https://doi.org/10.1175/MWR-D-12-00335.1.

——, D. S. Nolan, R. F. Rogers, and V. Tallapragada, 2015: Evaluating the impact of improvements in the boundary layer parameterization on hurricane intensity and structure forecasts in HWRF. *Mon. Wea. Rev.*, **143**, 3136–3155, https://doi.org/10.1175/MWR-D-14-00339.1.

Zhu, P., 2008: Simulation and parameterization of the turbulent transport in the hurricane boundary layer by large eddies. *J. Geophys. Res.*, **113**, D17104, https://doi.org/10.1029/2007JD009643.